Geometric Corrections in Coplanar Translational Laminography

Kai-Uwe THIESSENHUSEN[*], Uwe EWERT[*], Bernhard REDMER[*],
Klaus BAVENDIEK[**]
[*] BAM Bundesanstalt für Materialforschung, Berlin, Germany
[**] YXLON International, Hamburg, Germany

Abstract. Planar laminography is a method to obtain spatial information for objects whose geometrical dimensions disallow measurements with classical computed tomography. In coplanar translational laminography, the radiation source is moved relatively to the object and/or to the detector in a plane parallel to the detector plane. A 3D-image of the studied object can be reconstructed from the measured projections by filtered backprojection. Classical rotational tomographic scans include projections from all sides of an object from equidistant angles. In contrast, laminography is restricted by several distinct geometric limitations. This results in a number of artifacts interfering in the reconstructed image with real object structures. Projections obtained from different positions are not equally weighted because of the changing distance between radiation source and detector and due to different angles of incidence. A motion of the source in equidistant steps results in non equidistant angular steps which also influence the results. Especially, overshoots close to the boundaries of death angle zones disturb the resulting image of the object.
The influences of the different geometric effects on the results of a reconstruction process are discussed here. Several correction approaches to reduce the resulting artifacts are presented. These methods include several angular corrections applied at different steps in the filtering and reconstruction process. A number of artificial phenomena can be reduced considerably with these methods. SNR analysis is used for optimization of 3D-image quality

1. Introduction

Laminography is a method to obtain spatial information on objects where tomography is not possible, e.g. large planar objects or pipes. The observation of the object from different positions provides spatial information..

Unless tomography, laminography always describes an object incompletely. The most general restriction results from the fact that an object is studied within a limited angle range. This always leads to “blind angle“ phenomena.

Beside of this, a number of additional effects influence laminographic experiments. There are several different laminographic methods. We study here as an example the coplanar translational X-ray-laminography. Related problems, however, apply to other lamininographic scan geometries in a similar manner. In coplanar translational laminography, there is a linear motion of a radiation source device relatively to the studied object and the detector. The axis of source motion is parallel to the detector plane. The object is scanned and penetrated from a number of different angles.

The resulting 3D-matrix is generated from a number of filtered projections by a classical filtered backprojection procedure (FBP). The FBP algorithm is often preferred because of the significant higher reconstruction speed in comparison to algebraic reconstruction techniques (ART). The FBP is sensitive against any deviation from classical rotational computed tomography. This are irregularities due to non equidistant projection angle change and sensitivity changes due to different incident angles on the detector. Previous correction algorithms were based on a auto exposure correction.[1,2] For further applications e.g. in aerospace fields [3] higher accuracies are needed.

The filter procedure requires a large number of projections and typically produces "overshoots" at edges. At the borders of the "blind angle" region these overshoots do not compensate and produce artifacts in the 3D-image. The measured grey values strongly vary with the position of the radiation source. Therefore, different projections contribute in different quantities to the resulting image. The measurement geometry in an equidistant translational laminography leads to the situation, that the number of obtained data is varying for different incidence angles. In combination, these effects lead to additional artifacts.

In this work, we present an approach to quantify and reduces these artifacts. This enhances the reliability of laminographic measurements with respect to quantitative results in FBP procedures. It will also improve the data quality for algebraic reconstruction techniques (ART).

2. Intensity Effects

2.1 Observations

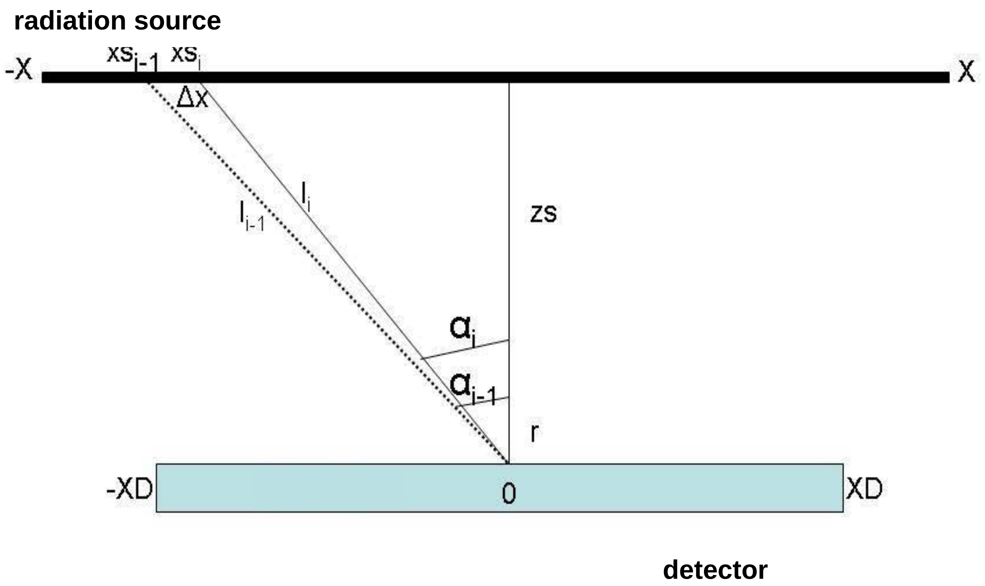

Figure 1. Measurement geometry. The radiation source moves along the upper axis in equidistant steps Δx, the detector is in the lower part of the image.

The geometry of a translational laminographic measurement is displayed in Fig.1. The radiation source moves along the upper axis. The detector is in a plane parallel to this axis in distance zs. The maximum source elongations are given by -X and X, respectively. Between these positions, the source moves in equidistant steps Δx.

The incidence angle α_i on the detector for the projection with index i is given by

$$\alpha_i = \arctan (xs_i / zs). \quad (1)$$

The distance l_i between source and detector center is

$$l_i = zs/\cos\alpha_i. \quad (2)$$

The values of l depend on α and therefore on the detector to source position. They are smallest for a "central projection", where the source is situated closest to the detector center (xs=0) and largest, when xs = -X or xs = X ("edge projection"). The grey values (or intensities) of the measured data directly depend on l. This has several reasons: at first, the radiation intensity I follows an inverse square law with distance from the source. This effect gives a contribution

$$I \sim l_i^{-2} \sim \cos^2\alpha_i. \quad (3)$$

Additionally, for some detectors, the intensities directly depend on the cosine of the angle of incidence on the detector surface. This angle is the same as α_i, so that a contribution of another $\cos\alpha_i$ must be taken into account.

If a planar object of thickness d being parallel to the detector is radiated, it causes an intensity attenuation proportional to $e^{-\mu d/\cos\alpha i}$. The attenuation coefficient μ depends on the material and on the radiation energy. These three contributions combined lead to

$$I \sim \cos^3\alpha_i\, e^{-\mu d/\cos\alpha i}. \quad (4)$$

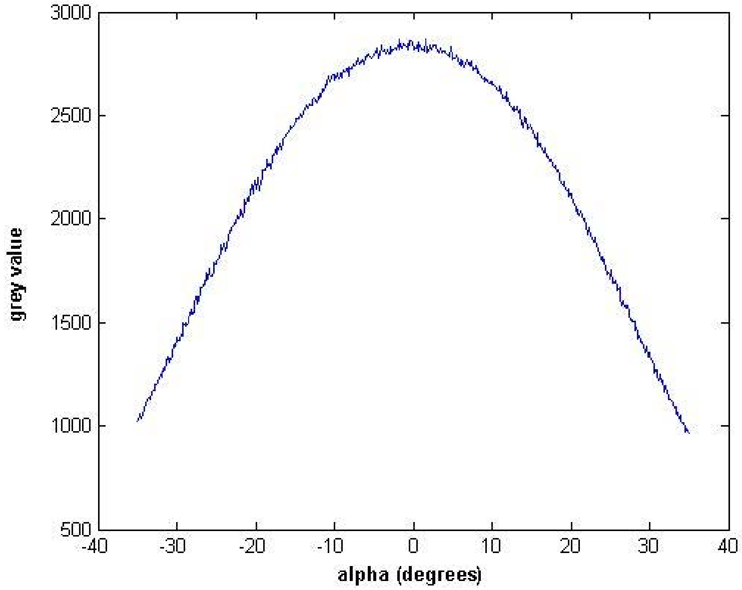

Figure 2. Measured grey values at the centre of the detector as function of incidence angle for 150 keV X-ray radiation after passing through a 7 mm thick steel plate.

In Fig. 2, an experimental illustration of these effects is shown. The measured intensity at the centre of a detector after transmitting through a 7 mm thick steel plate is plotted as function of the incidence angle. For angles of about 30°, the remaining intensity is about one third of that of the central projection.

These effects can also be observed within one and the same projection, especially for edge projections at low source to detector distances. When the distances between source and different parts of the detector are significantly different, it results in a “shading”. One example is given in Fig. 3., where an edge projection is displayed.

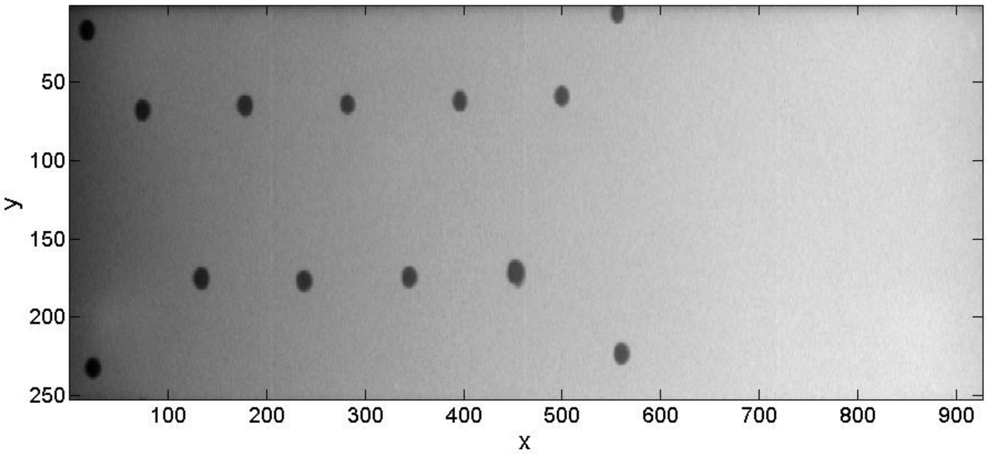

Figure 3. Edge projection (positive image) of a sample consisting of a number of lead particles on an acrylic glass plate combined with a homogeneous 7mm thick steel plate penetrated with X-rays at 150 keV. Parts with low intensities appear dark. The x and y scales are given in detector pixels, one pixel is 0.1 mm.

The sample displayed in this figure consists of a two parallel plates, an acrylic glass plate with a number of inserted small lead particles and a 7 mm thick homogeneous steel plate. To the right hand side, the intensity increases. The lead particles attenuate the radiation and appear dark.

2.2 Logarithmic Corrections

The intensity of radiation after passing through a section with length x of a material with an attenuation coefficient μ is

$$I = I_0 e^{-\mu x}. \qquad (5)$$

I_0 is the intensity of the unattenuated radiation and depends on several geometric factors explained above. For heterogeneous objects consisting of different materials $-\mu x$ in the exponent becomes the sum of different $-\mu_i x_i$. The x_i coefficients depend on the distribution of substances with different attenuations coefficients μ_i in the object. Taking the logarithms of these grey values, equation (5) becomes:

$$\ln I = \ln I_0 - \sum \mu_i x_i \qquad (6)$$

The equation decouples into two terms which can be studied separately. The first term, ln I_0, depends on the geometrical conditions of the measurement and changes only on long scales. The second term $\sum \mu_i x_i$ depends on the object properties.

In Fig. 4, the horizontal profiles of the grey values of two different projections of the same sample are plotted. The blue curve in the left image is a section from a horizontal profile through the edge projection displayed in Fig 3. The region around the four lead spheres in the lower part in Fig 3. (at y = 175) is plotted. The long scaled intensity increase is the shading effect.

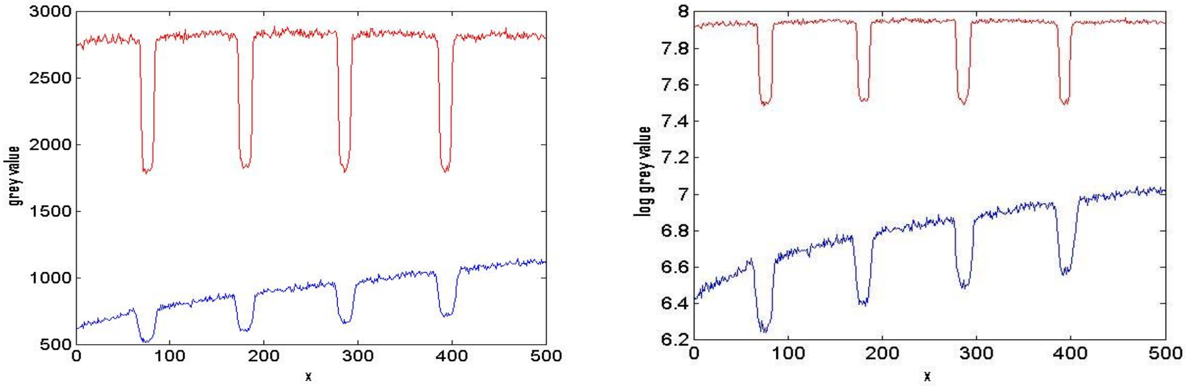

Figure 4. Left: horizontal profiles of original grey values of an edge projection (blue) and a central projection (red) across the line with four lead particles (y=175 in Fig. 3). Right: the corresponding logarithmic values. The x-unit is scaled in detector pixels, i.e. 0.1 mm.

The red curve in Fig. 4 is the corresponding central projection. Its intensity level is about three times larger, see Eq. (4) and Fig. 2. The intensity contrast at the lead spheres is proportional to the base intensities. The logarithms of these grey values are displayed in the right part of the figure. Here, the contrasts at the spheres does not depend on the absolute level of the grey values. When using the logarithms of the grey values of the projections, all off them contribute in a similar manner to the reconstruction result despite of their absolute intensity levels.

The noise levels, however, are still different. They are plotted in Fig. 5. In the original data (left), the fluctuations are larger for the central projection with larger intensity. This can be expected for a stochastic noise distribution which is proportional to the square root of the gray levels. For the logarithmic intensities, however, the noise for projections with low intensities is larger (lower right image).

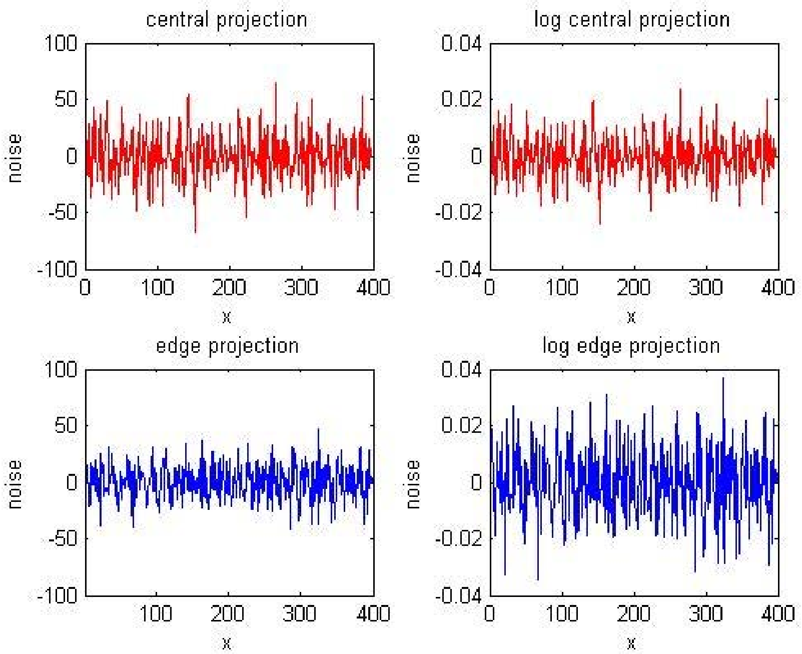

Figure 5. Left: noise level profiles of an edge projection (blue) compared with a central projection (red). Left from the original grey values, right from the logarithmic data. The x axis is scaled in pixel size (0.1 mm), the y-axis refer to the measured grey values and their logarithms.

3. Source Positioning Effects

3.1 Observations

When the radiation source moves in successive equidistant steps, the corresponding incident angles are necessarily not equidistant. This follows from the relation α = arc tan (xs /zs). For infinitesimally small steps dx, the relation between both quantities is:

$$d\alpha/dx = (d \arctan(xs/zs)/dx = \cos^2\alpha \ . \qquad (7)$$

The angular steps are thus smaller for larger α. Therefore, equidistant source motion provides more projections from larger incident angles, proportionally to $1/\cos^2\alpha$.

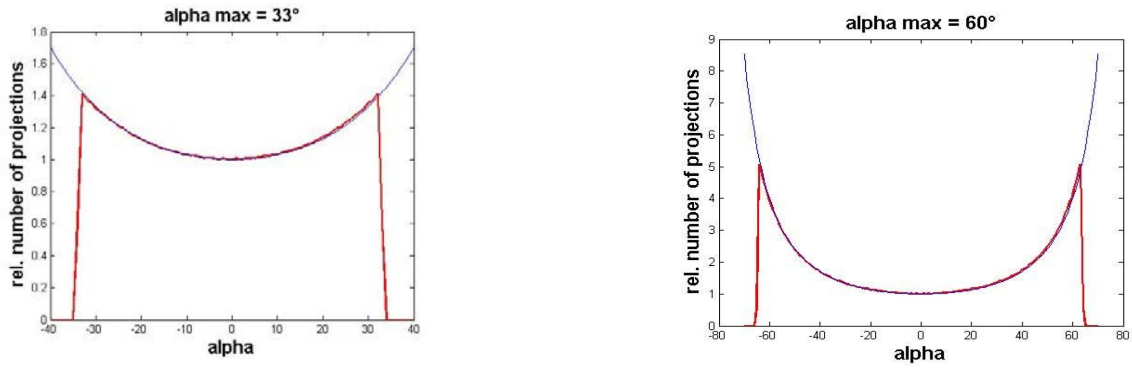

Figure 6. Red: relative number of projections per angle interval as function of incidence angle for a source motion in equidistant length steps. Left: for a maximum incidence angle of 33°, right of 60°. The y-values are normalized so that 1 is the value for α=0. Blue curves: $\cos^{-2}\alpha$.

Figure 6 illustrates the situation. The red curves show the relative number of projections per angle interval normalized so that the value 1 is for an incidence angle of zero; the blue curves are direct plots of $\cos^{-2}\alpha$. The left image is for a maximum incident angle of 33°. Here, the difference between outer and inner angular regions is small. In contrast to this, for a maximum incident angle of 60° (right), the relative number of projections per angular step is about five times larger than in the central region.

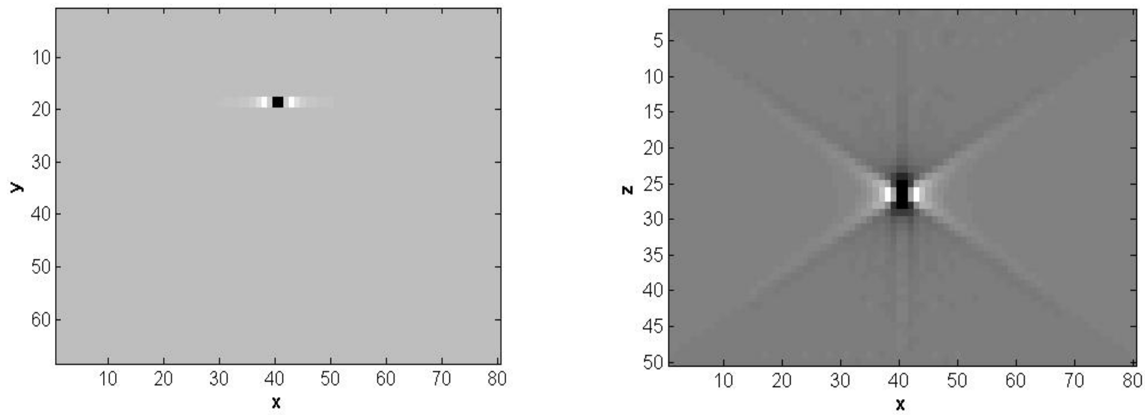

Figure 7. Reconstruction of a simulated attenuating object of 2x2x2 voxels (positive image). Left: x-y-display (parellel to the detector plane, x is scan direction), right: x-z display (z orthogonal to detector). The axes are scaled in voxel size units. The maximum incidence angle is 60°.

Fig. 7 shows as an example the reconstruction of a 2x2x2 voxel sized cube. The image is reconstructed from 500 projections simulated with the tool aRTist.[4] The left image shows an x-y-plot in a plane parallel to the detector. The object is the black square, the white fields beside it are filter artifacts. The right image shows the x-z direction, z is the direction between detector and the axis of source motion. Because of limited angle, there are blind angle sections left and right from the object. We focus here on additional artifacts just as overshoots at the borders of the blind angle areas.

3.2 Overshoot Correction

The overshoots result from two reasons: from the larger number of projections obtained from the edge regions as well as from the filtering procedure.

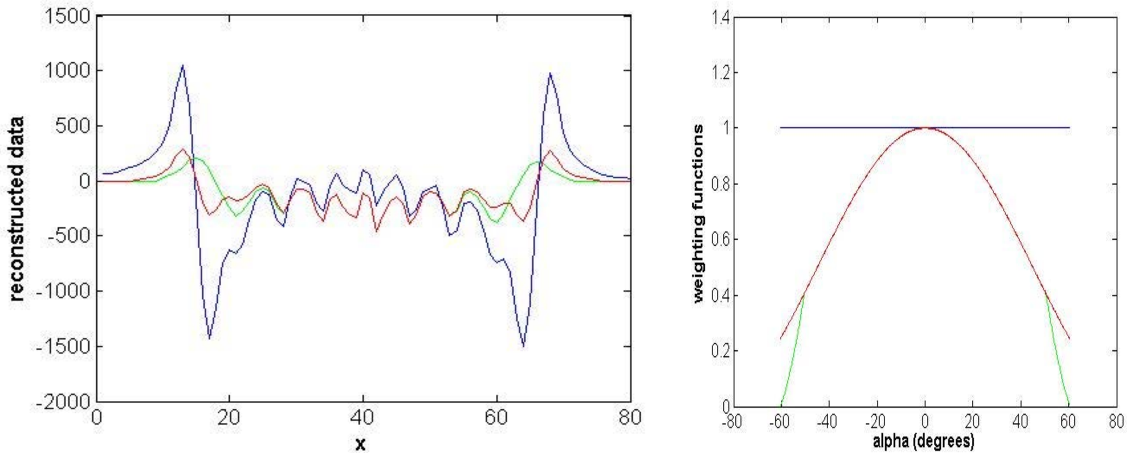

Figure 8. Reconstruction of a 2x2x2 voxel object. Left: three horizontal profiles through the x-z-reconstruction matrix (at z=40 in the right image of Fig. 7). Blue: original data, red data weighted by a cosine square function, green weighted by cosine square and an additional ramp function. The x unit is the voxel size. Right: the three corresponding weight functions as function of the incidence angle.

One example is given in Fig. 8. The blue curve in Fig. 8 is a horizontal profile through the set from the original data shown in Fig. 7 (right image) at z =40.

A data set from equidistant projection steps can simply be transformed into one from equal angular steps by multiplication of all projections with the $\cos^2$ of the incidence angle. This factor exactly compensates the enhanced number of projections obtained from larger angles. The result is shown in the red curve in Fig. 8, left. The overshoots are strongly reduced, and also the fluctuations in the inner part are smaller. This approach also reduces

This correction does not compensate the filter artifacts. Therefore, an additional weighting function is introduced. Here, the first and last 10% of the projections are weighted with the ramp function which is zero for the outermost projection and 1 for all in projections multiplied by the $\cos^2$-correction (green curve). This leads to an additional reduction of the overshoots. The right image shows the three corresponding weighting functions. Because the additional ramp function has influence only in the outer regions, the green and red curves are identical in the inner parts.

4. Summary

Several geometric effects influence the quality of laminographic reconstruction, especially with filtered backprojection algorithms. Projections from different incidence angles have significantly different intensity values (due to, e.g., the source-detector distance, the incidence angle on detector, shading). Using logarithmic data, these effects have no significant influence on reconstruction accuracy. Further intensity corrections are not necessary.

A tube positioning correction factor of cosine square of the incidence angle has been introduced. This correction term significantly reduces overshoots at the border of the "blind angle" region. An additional weighting function of the outermost projections leads to a further overshoot reduction.

The effects and correction methods described here for coplanar translational laminography can be different in detail for other laminographic geometries, but comparable algorithms are required too.

References

[1] Redmer, B., Ewert, U., Likhachov, A.V., Pickalov, V.V, Onel, Y., Li, Z., Baranov, V.A, Sensitive Detection of planar Defects by a Mechanised Radiometric Weld Inspection System, 15th World Conference on Nondestructive Testing. Roma (Italy) 15-21 October 2000

[2] Redmer, B., Robbel, J., Ewert, U., Vengrinovich, V., Mechanised weld inspection by tomographic computer-aided radiometry (TomoCAR), Insight 44 (9), p. 564-567 (2002)

[3] Ewert, U., Redmer, B., Raedel, C., Osterloh, K., Schnars, U., Henrich, R., Schimmelmann, O., Bavendiek, K., Jahn, M., Mobile X-ray inspection of light weight materials, Conference: International symposium on NDT in aerospace, Fürth (Germany), 3-5 Dec 2008; Proceedings, Deutsche Gesellschaft fuer Zerstörungsfreie Prüfung. Berichtsband v. 114.

[4] Jaenisch, G.-R., Bellon, C., Ewert, U., aRTist - Analytical RT Inspection Simulation Tool for Industrial Application, Proceedings of the 17th. World Conferences on Non-Destructive Testing, Shanghai, China, International Committee on NDT, 2008